

DOI: 10.1002/cssc.201301194

Cu₂O/Reduced Graphene Oxide Composites for the Photocatalytic Conversion of CO₂

Xiaoqiang An, Kimfung Li, and Junwang Tang^{*,[a]}

A facile one-step microwave-assisted chemical method has been successfully used for the synthesis of Cu₂O/reduced graphene oxide (RGO) composites. Photocatalytic CO₂ reduction was then investigated on the junction under ambient conditions. The RGO coating dramatically increases Cu₂O activity for CO₂ photoreduction to result in a nearly six times higher activity than the optimized Cu₂O and 50 times higher activity than the Cu₂O/RuO_x junction in the 20th hour. Furthermore, an apparent initial quantum yield of approximately 0.34% at 400 nm has been achieved by the Cu₂O/RGO junction for CO₂ photore-

duction. The photocurrent of the junction is nearly double that of the blank Cu₂O photocathode. The improved activity together with the enhanced stability of Cu₂O is attributed to the efficient charge separation and transfer to RGO as well as the protection function of RGO, which was proved by XRD, SEM, TEM, X-ray photoelectron spectroscopy, photo-electrochemical, photoluminescence, and impedance characterizations. This study further presents useful information for other photocatalyst modification for efficient CO₂ reduction without the need for a noble-metal co-catalyst.

Introduction

In the past decades, the significant rise in greenhouse gas CO₂ and the concern about the security of energy supply have received much attention and are regarded as the biggest challenges of the century. The conversion of CO₂ into useful chemicals or fuels by artificial photosynthesis has been considered as one of the most promising and compelling approaches to solve both energy and environmental problems simultaneously.^[1] Since the discovery of the photoreduction of CO₂ to form valuable chemicals by using semiconductors, many photocatalysts have been reported.^[2] However, the current CO₂ photoreduction efficiency is still very moderate. Generally, the fast recombination of charge carriers and the mismatch between the band gap of photocatalysts and solar radiation spectrum are the key factors that limit the efficiency of artificial photosynthesis.^[3,4] Many effective and low-cost photocatalysts such as TiO₂ are only sensitive to UV light, which only comprises a small fraction of solar energy that reaches the Earth's surface. The development of visible-light-driven semiconductors for artificial photosynthesis is a topic of great interest with practical importance.^[5]

Cuprous oxide, a direct-band-gap (2.0 eV) semiconductor, is an attractive p-type oxide for visible-light-driven artificial pho-

tosynthesis, such as photo-electrochemical water splitting.^[6,7] In theory, the narrow band gap and appropriate positioning of the conduction and valence bands also make it an ideal photocatalyst for CO₂ photoreduction.^[8,9] In our preliminary research, Cu₂O has been used for the photoconversion of CO₂ into CO, which is a value-added chemical for various synthetic reactions (e.g., Fischer–Tropsch synthesis) and significant fuel for energy generation. The selectivity and activity of Cu₂O crystals was improved by controlling the facets that were exposed and loading RuO_x as a co-catalyst.^[10] Furthermore, we found that the spherical aggregates suppressed unexpected H₂ production to improve CO₂ reduction. However, the stability of Cu₂O is a serious issue as the redox potentials for the reduction and oxidation of monovalent copper oxide lie within the band gap.^[11] In addition, the activity of the photocatalyst for CO₂ reduction is quite moderate. Thimsen et al. reported recently that Cu₂O with Al-doped zinc oxide and titanium oxide as protective layers improved the photostability of Cu₂O for photo-electrochemical water splitting.^[11] Therefore, we attempt to improve both the stability and activity of the Cu₂O for CO₂ photoreduction by making an efficient junction composite, which is highly desirable for artificial photosynthesis in a sustainable manner.

As a result of the promising electronic and catalytic properties, carbonaceous nanomaterials have been utilized extensively to improve the performance of photocatalysts.^[12] For example, the presence of a thin protective carbon layer could remarkably improve the photostability as well as photocurrent density of cuprous oxide nanowire arrays.^[13] Graphene, a 2D monolayer of sp²-hybridized carbon atoms, has attracted intense attention in recent years because of its excellent physical and chemical properties. There is an increasing interest in the rational design of graphene-based photocatalysts for solar fuel production, and these are usually prepared by the reduction of

[a] X. An, K. Li, Dr. J. Tang
Department of Chemical Engineering
University College London
London, WC1E 7JE (United Kingdom)
E-mail: Junwang.tang@ucl.ac.uk

 Supporting Information for this article is available on the WWW under <http://dx.doi.org/10.1002/cssc.201301194>.

 © 2014 The Authors. Published by Wiley-VCH Verlag GmbH & Co. KGaA. This is an open access article under the terms of the Creative Commons Attribution Non-Commercial License, which permits use, distribution and reproduction in any medium, provided the original work is properly cited and is not used for commercial purposes.

graphene oxide (commonly referred to as RGO). However, few graphene-based materials, for example, those bonded with the wide-band gap materials TiO_2 , WO_3 , and Ta_2O_5 , have been developed for the photoreduction of CO_2 , although there are several reports on photocatalytic water splitting because of the extreme thermodynamic inertness of CO_2 .^[14–17] A graphene-containing narrow-band-gap photocatalyst is thus highly desirable for CO_2 photoreduction, which has been less reported. With a combination of the potential advantages of Cu_2O and RGO, $\text{Cu}_2\text{O}/\text{RGO}$ composites were targeted in our study, which could be attractive as visible-light-driven CO_2 reduction catalysts in which RGO can not only act as an ideal electron trap to hinder fast charge recombination but also as a stabilizer to improve the stability of Cu_2O .^[18]

Herein, for the first time we demonstrated a microwave-assisted method for the fabrication of $\text{Cu}_2\text{O}/\text{RGO}$ composites, which were used for CO_2 photoconversion. As a result of the efficient interfacial charge separation and transfer, $\text{Cu}_2\text{O}/0.5\%$ RGO composites exhibit a high efficiency for photocatalytic CO_2 conversion without the need for a noble-metal co-catalyst. The stability of the photocatalysts is also improved remarkably by coupling with RGO and shows a linear relationship between the reaction activity and reaction time. The reason behind the enhancement was also investigated and is discussed.

Results and Discussion

As proved in our previous study, spherical Cu_2O aggregates (cuboid microstructure) characterized by exposed $\{100\}$ facets are better for CO_2 conversion than octahedral Cu_2O particles characterized by exposed $\{111\}$ facets.^[8] The spherical Cu_2O aggregates are referred to herein as the photocatalysts. The XRD patterns of spherical Cu_2O and $\text{Cu}_2\text{O}/\text{RGO}$ composites both prepared by an identical one-step microwave-assisted chemical route are shown in Figure 1. All the diffraction peaks in the XRD patterns of both samples match well with those of cubic-phase Cu_2O (JCPDS No.78-2076). For $\text{Cu}_2\text{O}/\text{RGO}$ composites, no peaks that correspond to RGO, Cu, CuO, or $\text{Cu}(\text{OH})_2$ were detected. The absence of diffraction peaks of carbon species is

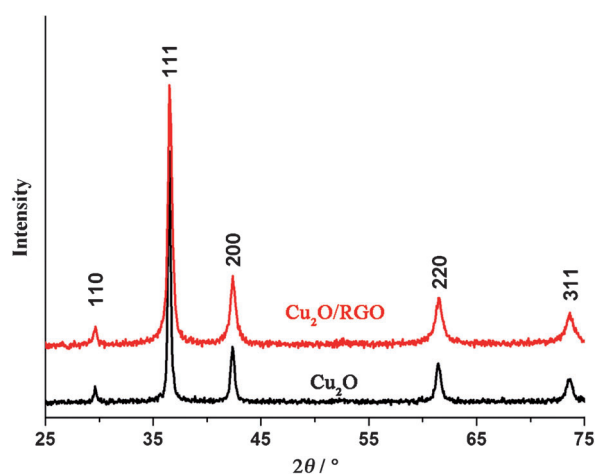


Figure 1. XRD patterns of Cu_2O and $\text{Cu}_2\text{O}/\text{RGO}$ composites.

attributed to the low amount and the relatively low diffraction intensity of RGO.^[19]

The morphology of Cu_2O and $\text{Cu}_2\text{O}/\text{RGO}$ composites was investigated by SEM and TEM. Blank Cu_2O presents a typical morphology of spherical aggregates with an average diameter of approximately $5\ \mu\text{m}$ (Figure 2a). The morphology of exfoliat-

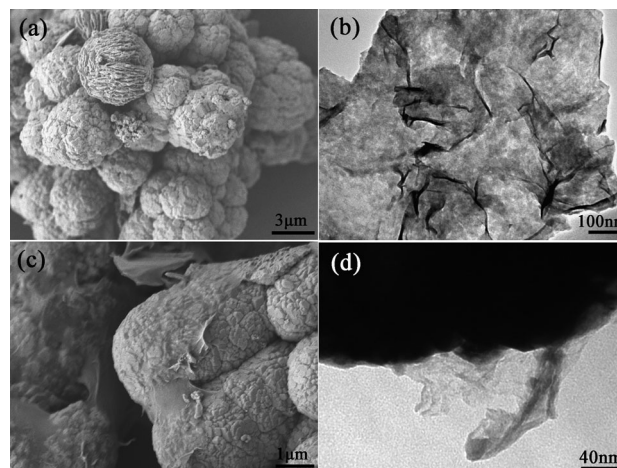


Figure 2. (a) SEM image of Cu_2O microspheres. (b) TEM image of graphene oxide. (c) SEM image of $\text{Cu}_2\text{O}/\text{RGO}$ composites. (d) TEM image of $\text{Cu}_2\text{O}/\text{RGO}$ composites.

ed GO sheets, which are used as precursor to fabricate $\text{Cu}_2\text{O}/\text{RGO}$ composites, is shown in Figure 2b. The thin sheet shows a typical 2D structure with many wrinkles and folds. In most cases, the introduction of RGO has a negligible influence on the morphology of the product. The flexible RGO sheets can be observed clearly on the surface of the spherical aggregates, which indicates the formation of $\text{Cu}_2\text{O}/\text{RGO}$ composites (Figures 2c and S1a). As reported, the formation of $\text{Cu}_2\text{O}/\text{RGO}$ aggregates is a result of the strong affinity between the metal oxide and the abundant functional groups of graphene oxide.^[18,20] The intimate contact between the RGO sheet and Cu_2O microspheres was further confirmed by TEM (Figure 2d).

The structures of the as-prepared photocatalysts were characterized by X-ray photoelectron spectroscopy (XPS; Figure S1b). To investigate the degree of reduction of GO in the reduction process, high-resolution C 1s XPS spectra were collected from $\text{Cu}_2\text{O}/\text{RGO}$ composites (Figure 3a). The C 1s spectrum can be deconvoluted into three peaks at 284.6, 285.8, and 288.7 eV, which are associated with graphitic sp^2 carbon ($\text{C}=\text{C}/\text{C}-\text{C}$), carbonyl ($\text{C}=\text{O}$), and carboxyl ($\text{O}=\text{C}=\text{O}$) functional groups, respectively.^[21] The relative content of graphitic carbon in the sample is estimated to be 69.6%, which is much higher than 41.9% of GO.^[22] The much stronger peaks related to graphitic sp^2 carbon suggests considerable deoxygenation in the one-step hydrothermal reaction, which leads to the formation of RGO in the composites. The fitted Cu 2p spectra of Cu_2O and $\text{Cu}_2\text{O}/\text{RGO}$ composites are shown in Figure 3b and c, respectively, which assists the determination of the oxidation states of Cu elements. In the asymmetric core-level spectrum, the peaks at 932.4 and 952.2 eV correspond to the binding

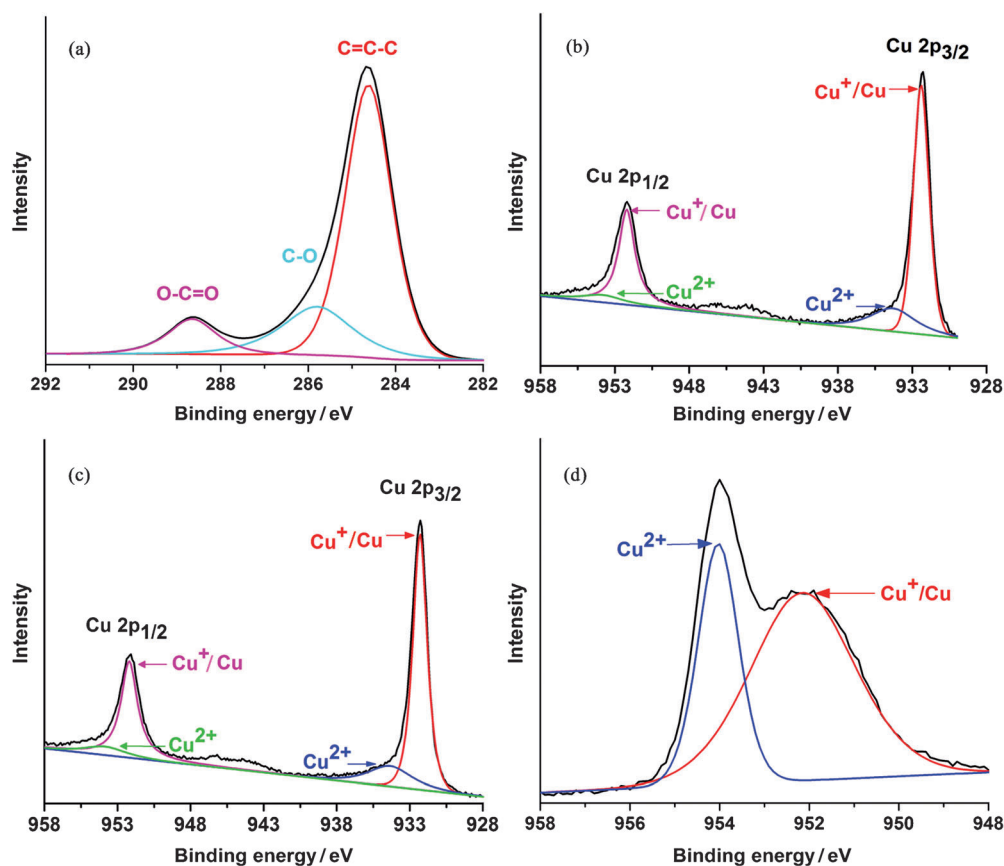


Figure 3. (a) C 1s spectrum of $\text{Cu}_2\text{O}/\text{RGO}$ composites. (b) Cu 2p spectrum of Cu_2O . (c) Cu 2p spectrum of $\text{Cu}_2\text{O}/\text{RGO}$ composites. (d) Cu 2p spectrum of Cu_2O treated under air atmosphere.

energy of $\text{Cu}2p_{3/2}$ and $\text{Cu}2p_{1/2}$ of Cu_2O or Cu, and those at 934.3 and 953.8 eV are attributed to CuO .^[23] The appearance of weak and broad satellite peaks around 943.0 eV also confirms the coexistence of a trace amount of CuO , although it is not detected in the XRD measurements.^[24] This can be ascribed to the relatively small amount and the amorphous nature of CuO that might be because of surface oxidization of Cu_2O .

The activity of samples for the photoreduction of CO_2 was then evaluated at ambient temperature under 150 W Xe lamp irradiation. To exclude the possible influence of contaminants on the solid composite photocatalyst, a thermal pretreatment was performed before each photocatalytic test. Based on the control photocatalytic experiment under identical conditions but in the absence of CO_2 ($\text{Cu}_2\text{O}/0.5\%$ RGO composites under Ar atmosphere), the negligible amount of CO (Figure S2a) indicates that the surface of the photocatalysts is clean and RGO cannot be converted to CO under these experimental conditions. Furthermore, no obvious CO is detected either in the absence of light or photocatalyst (Figure S2a). The activity of Cu_2O and $\text{Cu}_2\text{O}/\text{RuO}_x$ samples was tested firstly, with a thermal pretreatment in air similar to that reported before.^[10] The evolution of CO is detected as the major product if spherical Cu_2O aggregates are used as the photocatalyst without a noble-metal co-catalyst (Figure 4a), in agreement with the previous report.^[10] Cu_2O treated in air, $\text{Cu}_2\text{O}/\text{RuO}_x$ treated in air, and Cu_2O treated in Ar show different activities. The amount of CO

produced by Cu_2O treated in Ar is at least three times greater in 2 h compared with the sample treated in air. The difference is because of the amount of CuO , which is much higher in the latter than the former as proved later. As we recently also found that the active component for H_2 production in a $\text{Cu}_x\text{O}/\text{TiO}_2$ junction is Cu_2O rather than CuO ,^[25] it is informative to evaluate the ability of CuO for CO_2 photoreduction.

A similar microwave-assisted hydrothermal reaction was used to fabricate a CuO photocatalyst. Less than 10 ppm CO is detected after 6 h (Figure S2b), which is much poorer than any Cu_2O -based photocatalyst. It is clear that RGO exhibits a significant influence on the yield of CO as even a small amount of RGO leads to a twofold enhancement in the reaction activity. The $\text{Cu}_2\text{O}/0.5\%$ RGO composites produce CO at an average of $50 \text{ ppm g}^{-1} \text{ h}^{-1}$ nearly linearly for 20 h.^[26,27] This average value is approximately one order of

magnitude higher than that of Cu_2O treated under air and even four times higher than the $\text{Cu}_2\text{O}/\text{RuO}_x$ junction reported previously. We also measured possible products, for example, methanol, in solution but did not find other product except CO (Figure S3). To clarify the origin of the CO generated during the reaction, the photoreduction of ^{13}C -labeled CO_2 was conducted by using the $\text{Cu}_2\text{O}/\text{RGO}$ photocatalyst. Negligible ^{12}CO ($m/z=28$) is observed in the mass spectrum (Figure 4c). The dominant peak of ^{13}CO ($m/z=29$) clearly indicates that the evolved CO originates entirely from the photoreduction of ^{13}C -labeled CO_2 rather than organic contaminants that might be adsorbed on the photocatalyst surface or in the reactor if $\text{Cu}_2\text{O}/\text{RGO}$ is used as the photocatalyst.^[28,29] Furthermore, we compared $\text{Cu}_2\text{O}/\text{RGO}$ with P25 TiO_2 for CO_2 conversion under the full arc irradiation of a 150 W Xe lamp. $\text{Cu}_2\text{O}/\text{RGO}$ exhibits at least 20 times higher activity than P25 TiO_2 under identical experimental conditions (Figure 4d).^[15]

The composite was also optimized as shown in Figure 4b. An appropriate loading amount of RGO is crucial to achieve the best photocatalytic activity, which is 0.5% RGO. Less RGO cannot separate electrons from holes efficiently, and more RGO would block light absorption.^[30] The optical absorption of the photocatalysts was investigated accordingly. Interestingly, the absorption ability of Cu_2O is relatively enhanced in both the UV and visible regions if coupled with 0.5% RGO (Figure 5a). As a result of the very thin layer of RGO synthesized, we

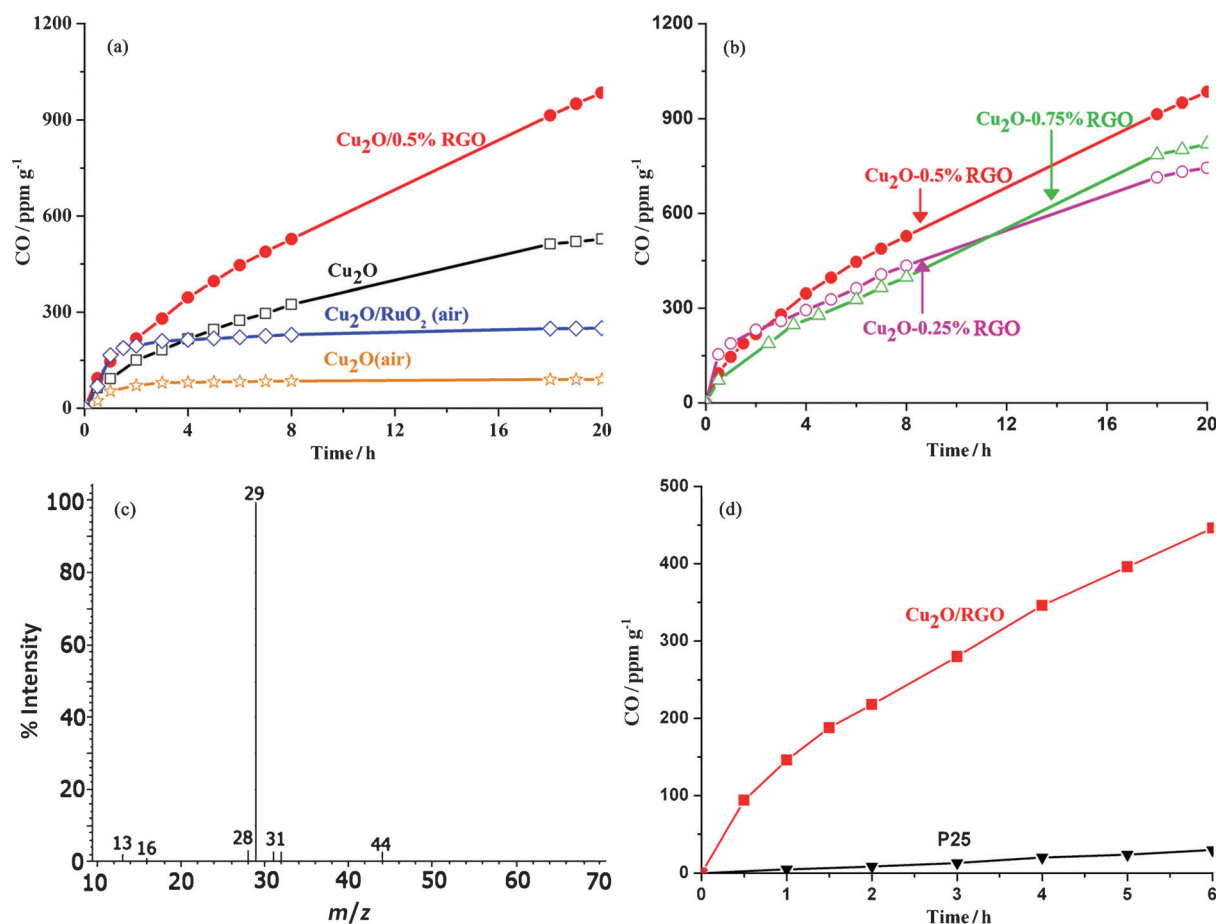


Figure 4. (a) Time-dependent photocatalytic conversion of CO₂ into CO over Cu₂O and Cu₂O/RGO composites. (b) Photocatalytic conversion of CO₂ over Cu₂O/RGO composites with different amounts of RGO (0.5 g photocatalysts, sodium sulfite as a hole scavenger, full arc irradiation of a 150 W Xe lamp). (c) MS spectrum of the gas-phase products of ¹³CO₂ photoreduction by the Cu₂O/RGO photocatalyst. (d) Time-dependent photocatalytic conversion of CO₂ over Cu₂O/RGO and P25.

cannot attribute the enchanted absorption to RGO absorption only. This might be because of the scattering of the RGO layer to Cu₂O. Compared to blank Cu₂O, a slight redshift of the light absorption edge is also observed, which could be attributed to the hybridization of the carbon material.^[30,31] As a result, the band gap of the Cu₂O/RGO composites is estimated to be 1.94 eV, which is somewhat smaller than that of Cu₂O (1.98 eV).

To prove the impact of RGO on the separation and transport of photogenerated charge carriers, photocurrent measurements were performed by depositing these materials on fluorine-doped tin oxide (FTO) electrodes. The fast and reproducible photocurrent response for each switch-on and switch-off light cycle in both p-type Cu₂O (treated in Ar) and Cu₂O/RGO electrodes is shown in Figure 5b. Under irradiation, the photocurrent of the Cu₂O/RGO electrode is approximately 1.6 times higher than the blank Cu₂O electrode prepared in Ar, which is consistent with the results of CO₂ photoconversion. As the photocurrent is dominated by electron transfer in the p-type photoelectrodes, the enhanced photocurrent can be regarded as straightforward evidence for the improved separation of electrons from holes in Cu₂O. The trapped electrons in RGO can be transferred readily to the FTO conductive glass because

of the Ohmic contact between them, which minimizes charge recombination losses.^[32]

The effect of RGO on the stability of Cu₂O during the photocatalytic reaction is clear. Photocatalysts treated under an air atmosphere suffer a dramatic decrease of CO production within the first hour. Differently, the profile of the composite activity is a nearly linear increase that can be maintained for more than 20 h. To further indicate the stability issue, the yields of CO in the 20th hour over different photocatalysts are shown in Figure 6a. As can be seen, 46 ppm g⁻¹ CO is produced over Cu₂O/0.5% RGO, which is 5.7 times higher than that of blank Cu₂O (8 ppm g⁻¹). Compared to Cu₂O treated in air and Cu₂O/RuO_x (both less than 1 ppm g⁻¹), more than 50 times enhancement has been achieved. The poor stability of Cu₂O and Cu₂O/RuO_x treated under an air atmosphere is attributed to the partial oxidation of CuO upon heating. The XPS peak that corresponds to Cu²⁺ is much higher than that in the Cu₂O sample treated under an Ar atmosphere (Figure 3d). As a result of the more positive conduction band of CuO, the relatively high amount of CuO inevitably results in deteriorated photocatalytic activity for CO production, which agrees well with previous results.^[25,33]

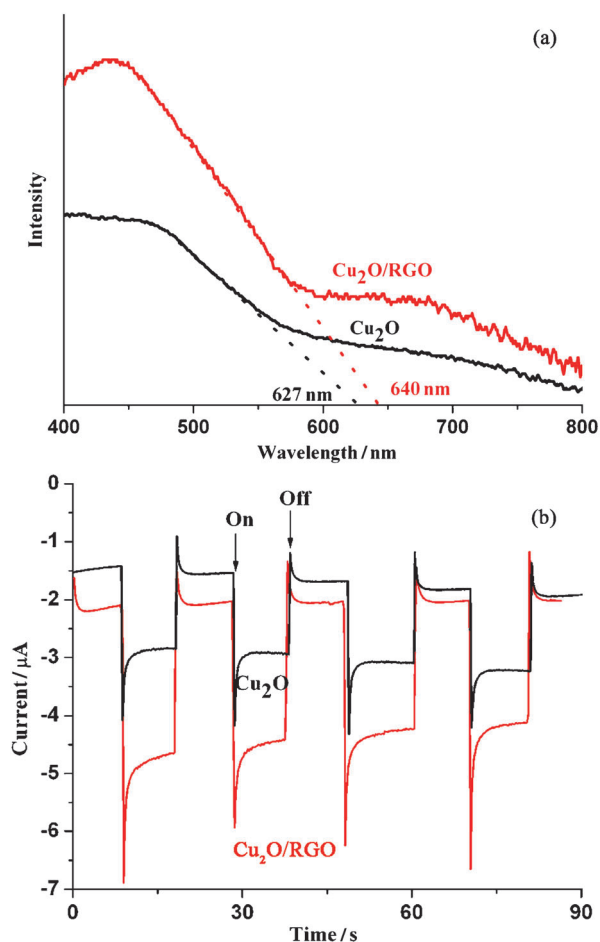


Figure 5. (a) UV/Vis spectra of Cu_2O and $\text{Cu}_2\text{O}/0.5\%$ RGO composites. (b) Photocurrent response of Cu_2O and $\text{Cu}_2\text{O}/\text{RGO}$ electrodes (full spectrum, 150 W Xe lamp, 0.5 M NaSO_4 solution, pH = 6.8).

To investigate the structural changes of Cu_2O under irradiation, Cu_2O treated under Ar and $\text{Cu}_2\text{O}/0.5\%$ RGO were collected after the photoreduction reaction and characterized by XPS and XRD measurements. The XPS spectra of Cu_2O and $\text{Cu}_2\text{O}/0.5\%$ RGO composites after the photocatalytic reaction are shown in Figure S4. Compared with the data shown in Figure 3b and c, the partial transformation of Cu_2O into CuO is confirmed by the increased peak intensities that correspond to CuO. These results indicate that the activity and stability of Cu_2O -based photocatalysts during CO_2 photoreduction show a strong dependence on the oxidation state of Cu. RGO can protect the Cu_2O surface from oxidation as indicated by XPS measurements, which is similar to a Cu_2O nanowire coated with a carbon layer for efficient water reduction.^[13] Furthermore, the reduction of Cu^+ into Cu metal is the other issue that influences the photocatalyst activity and stability, which cannot be identified easily by XPS. In the XRD pattern of Cu_2O after the photocatalytic reaction (Figure 6b), two additional peaks at around 43.3° and 50.4° are observed, which can be indexed to Cu metal (JCPDS No. 04-0836). The appearance of Cu metal indicates concomitant light-induced reduction reaction under irradiation. However, no peak that corresponds to Cu is

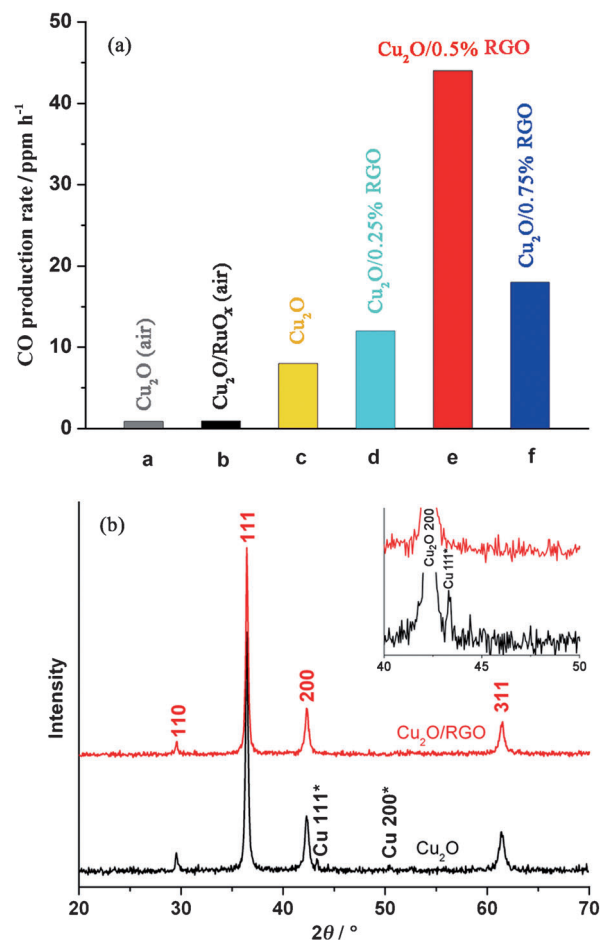


Figure 6. (a) CO yield in the 20th hour over different photocatalysts. (b) XRD patterns of Cu_2O and $\text{Cu}_2\text{O}/\text{RGO}$ after the photocatalytic reaction.

detected in the $\text{Cu}_2\text{O}/\text{RGO}$ composites after the reaction. It is reasonable that the efficient electron transfer from Cu_2O to RGO results in the inhibited reduction of Cu^+ , which also improves the stability of the photocatalyst.

Leaching experiments are usually used to evaluate photocorrosion during a photocatalytic reaction. The leaching of Cu from the photocatalysts was studied by analyzing the change of concentration of Cu ions in the solution by using inductively coupled plasma optical emission spectrometry (ICP-OES). The leaching of Cu caused by photocorrosion is only 96 ppm for $\text{Cu}_2\text{O}/\text{RGO}$ (Figure 7a). However, Cu_2O suffers much more serious photocorrosion with a value of 2670 ppm after 3 h. These results agree well with the inconspicuous morphological change of $\text{Cu}_2\text{O}/\text{RGO}$ photocatalysts (Figure S5). Furthermore, $\text{Cu}_2\text{O}/\text{RGO}$ composites exhibit reproducible activity during four consecutive runs (Figure S6).

Electrochemical impedance spectroscopy (EIS) was used to study the influence of RGO on the conductivity and charge transfer of the materials. The Nyquist plot of $\text{Cu}_2\text{O}/0.5\%$ RGO has a much smaller radius than that of blank Cu_2O (Figure 7b). As reported, the semicircle in a Nyquist plot at high frequencies is characteristic of the charge transfer process and the di-

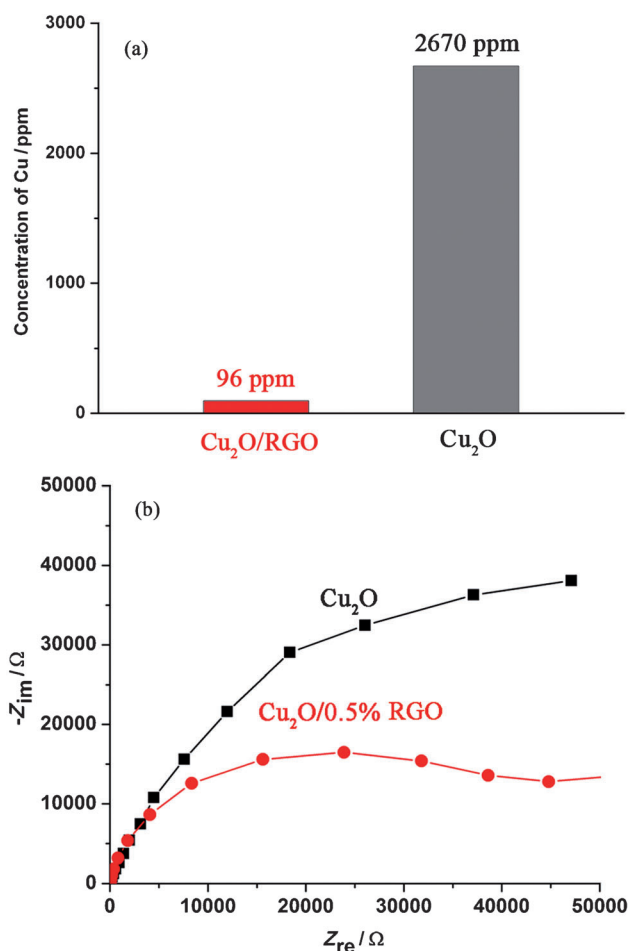


Figure 7. (a) Leaching of Cu caused by photocorrosion after 3 h reaction time. (b) EIS of Cu₂O and Cu₂O/RGO composite electrodes.

iameter of the semicircle is an indicator of the charge transfer resistance.^[34] The smaller resistance of Cu₂O/RGO composites further confirms that the thin layer of RGO with good conductivity does not block electron transfer but facilitates electron migration to the reaction sites on the surface of the composite.

Mott–Schottky analysis was used to determine both the donor density and flat-band potential (E_{FB}) at the semiconductor–liquid interface. Both Cu₂O and Cu₂O/RGO show a negative slope (Figure 8a), which indicates p-type semiconductor properties.^[35] The sample with 0.5% RGO exhibits a smaller slope in the Mott–Schottky plot than blank Cu₂O, which suggests an increase of donor density. The flat-band potentials of Cu₂O and Cu₂O/0.5% RGO, calculated from the x intercepts of the linear region, are -0.11 and -0.08 V vs. Ag/AgCl, respectively. Generally, the potential measured against an Ag/AgCl reference can be converted into normal hydrogen electrode (NHE) potentials by using Equation (1):^[36]

$$E_{FB(\text{vs. NHE})} = E_{FB(\text{pH } 0, \text{ vs. AgCl})} + E_{AgCl} + 0.059 \times \text{pH} \quad (1)$$

The measured pH value of the electrolyte is approximately 6.8, and $E_{AgCl} = 0.197$ V. Therefore, the calculated flat-band posi-

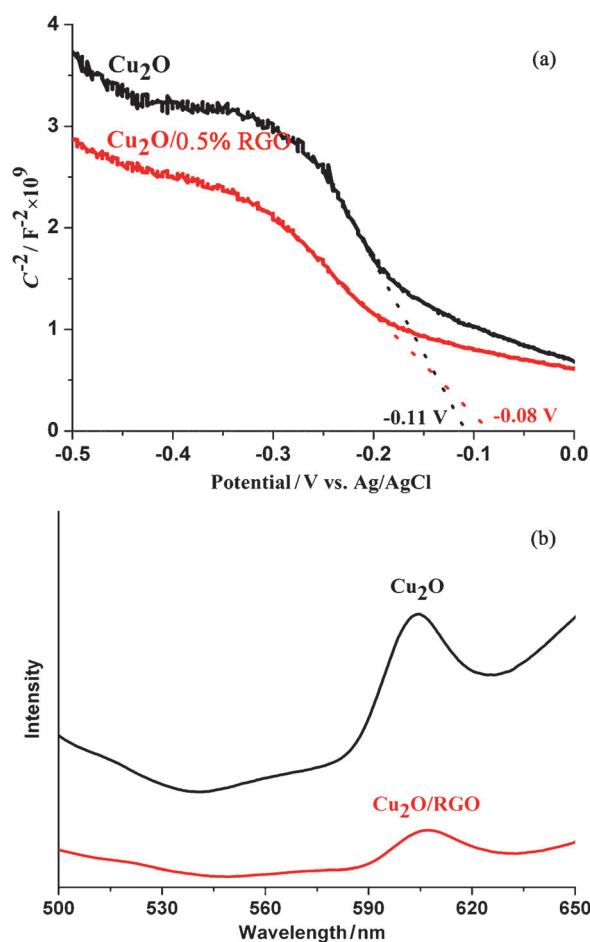
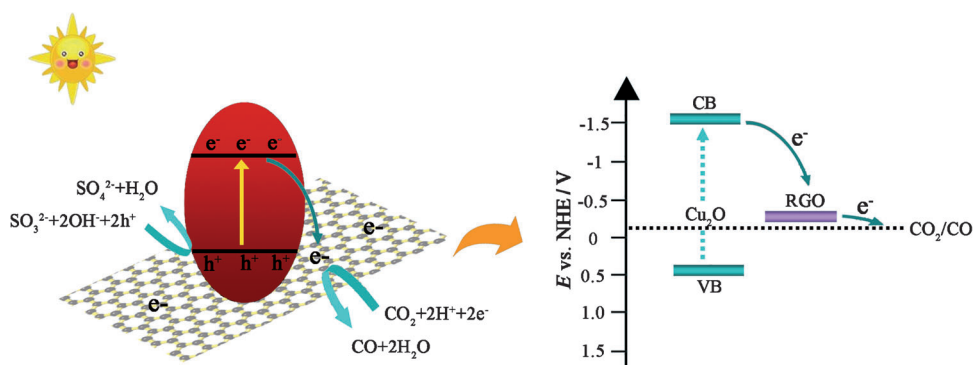


Figure 8. (a) Mott–Schottky plots of Cu₂O and Cu₂O/RGO. (b) PL spectra of Cu₂O and Cu₂O/RGO.

tions of Cu₂O and Cu₂O/RGO are 0.47 and 0.5 V vs. NHE (pH 0), thus the wrapping of Cu₂O by RGO has little influence on the potential of the photogenerated holes.^[37] The influence of RGO on the recombination of electron–hole pairs was further confirmed by photoluminescence (PL) measurements, which are widely used to study the efficiency of charge-carrier trapping, migration, and transfer in photocatalysts. The PL spectra of Cu₂O and Cu₂O/RGO composites under an excitation wavelength of 400 nm are presented in Figure 8b. Cu₂O shows a broad PL emission peak at around 605 nm. As expected, Cu₂O/RGO shows an extremely reduced PL intensity, which indicates the mitigated charge recombination in comparison to Cu₂O.^[38] Generally, this is attributed to the efficient charge transfer from Cu₂O to RGO, which leads to an improvement in the separation efficiency of the light-stimulated carriers.^[39] Following the significantly improved photocatalytic activity and stability, the apparent quantum yield of Cu₂O/RGO was measured in the visible region to be approximately 0.34% at 400 nm.

Based on these results, the reasons for the superior photocatalytic activity and stability of Cu₂O/RGO during noble-metal-free CO₂ reduction are illustrated in Scheme 1. The electronic structures of Cu₂O and RGO are discussed first. With a band



Scheme 1. Schematic illustration of the charge transfer in $\text{Cu}_2\text{O}/\text{RGO}$ composites.

gap of 1.94 eV and a valence band at around 0.5 eV, the conduction band of Cu_2O in the composites is estimated to be -1.44 eV vs. NHE (pH 0). RGO, with superior conductivity, can enhance the charge separation significantly, which is crucial for the electron-dominated reduction reaction.^[39,40] Secondly, with a lower activation potential and more active sites for the photoreduction reaction, RGO is considered as a promising 2D substrate for solar fuel production compared to others reported for water splitting.^[41] Furthermore, it has been reported that the restrained accumulation of electrons and decreased local electron density in graphene-based composites can facilitate the two-electron interaction for CO production selectively.^[42] Finally, the role of RGO as an electron acceptor that can extract electrons from Cu_2O retards the possible reduction of Cu_2O efficiently and improves photostability of the photocatalyst significantly.^[43] Furthermore, the presence of the RGO layer also prevents the direct contact of Cu_2O with water, which slows the oxidation of Cu_2O into CuO .^[44]

Conclusions

A microwave-assisted in situ reduction chemical method has been used to fabricate $\text{Cu}_2\text{O}/\text{reduced graphene oxide (RGO)}$ junction composites for the photocatalytic reduction of CO_2 . By coupling with RGO, the photoreduction activity of Cu_2O was enhanced by two times, with CO as the only reduction product. Furthermore, an almost linear reactivity for CO_2 conversion has been achieved, which represents an approximately six times increase of the CO production rate in the 20th hour compared with blank Cu_2O to result in an apparent quantum yield of approximately 0.344% in the visible region (at 400 nm). Stability is an issue for a Cu_2O photocatalyst. The incorporation of RGO into Cu_2O improves the photocatalyst stability remarkably, which shows a great potential for CO_2 conversion in a sustainable manner. Based on the optical and electrochemical measurements, the superior photocatalytic activity and stability of $\text{Cu}_2\text{O}/\text{RGO}$ composites are ascribed to the retarded electron-hole recombination, efficient charge transfer, and protective function of RGO. This work opens a promising prospect for the utilization of $\text{Cu}_2\text{O}/\text{RGO}$ as a visible-light-

driven photocatalyst for CO_2 photoconversion without the need for a noble-metal co-catalyst.

Experimental Section

Synthesis of $\text{Cu}_2\text{O}/\text{RGO}$ junction composites

Graphene oxide (GO) solution was synthesized from natural graphite powder by a modification of Hummers' method.^[45] $\text{Cu}_2\text{O}/\text{RGO}$ composites were fabricated by a microwave-assisted hydrothermal reaction. Firstly, $\text{Cu}(\text{NO}_3)_2$ was added to a mixture of ethanol and water in the ratio of 64:36. Then, a calculated amount of GO solution and formic acid (3 mL) were added. For optimization, $\text{Cu}_2\text{O}/\text{RGO}$ composites with different amounts of RGO were also synthesized, which include $\text{Cu}_2\text{O}/0.25\%$ RGO, $\text{Cu}_2\text{O}/0.5\%$ RGO, and $\text{Cu}_2\text{O}/1\%$ RGO, in which $x\%$ represents the calculated weight ratio of the GO added to Cu_2O . After stirring for 2 h, the homogeneous solution was heated with stirring in the microwave system at 150°C for 3 h. After the product was cooled to RT, the final product was collected by centrifugation, washed with water five times, and dried at 70°C . Blank Cu_2O was synthesized through the same procedure, except for the addition of GO solution.

Characterization

XRD was performed by using a Rigaku RINT 2100 diffractometer at a voltage of 40 kV. The morphologies of the products were characterized by field-emission scanning electron microscopy (FESEM, JEOL-6701F) and TEM (JEOL-2010F). UV/Vis spectra were recorded by using a Shimadzu UV/Vis 2550 spectrophotometer. XPS measurements were performed by using a Thermo Scientific XPS spectrometer. PL emission spectra were measured at RT by using a fluorescence spectrophotometer (F-4500, Hitachi).

Fabrication of film electrodes and electrochemical measurements

Photocatalyst (5 mg) and Nafion solution (10 μL , 5 wt%) were dispersed in a water/isopropanol mixture (1 mL, 3:1 v/v) by at least 30 min sonication to form a homogeneous catalyst colloid. For the measurements, the catalyst colloid (100 μL) was deposited onto an area of approximately 1 cm^2 of the FTO conductive glass to form the working electrode. A Pt wire was used as a counter electrode, and an Ag/AgCl electrode was the reference electrode in the three-electrode photo-electrochemical system. The electrolyte was 0.5 M NaSO_4 aqueous solution degassed with Ar. Electrochemical measurements were performed by using an Iviumstat potentiostat equipped with Ivium software. EIS were recorded under an alternating current perturbation signal of 10 mV over the frequency range of 1 MHz to 100 mHz. Mott-Schottky plots were obtained under direct current potential polarization. The potential ranged from -1.0 to 0 V with a potential step of 10 mV at a frequency of 1 kHz.

Photocatalytic activity measurements

The CO₂ reduction reaction was performed in batches by using a septum-sealed glass chamber with a volume of 120 mL, which was heated at 160° for 1 h prior to measurement. To remove possible trace organic contaminants, photocatalysts were treated at 200 °C for 3 h in a tubular furnace under the protection of Ar or in air (denoted Cu₂O treated in Ar or air). A typical photocatalytic experiment was conducted by using 0.5 g of photocatalysts and 3 mL of deionized water in a CO₂-purged 120 mL reactor. Excess (0.7 M) sodium sulfite was added to each batch as a hole scavenger.^[15,46] A 150 W Xe lamp (Newport) was used as a light source. The light output was measured by using a Newport 1918-R high-performance optical power meter fitted with a Newport 918-D calibrated photodetector equipped with an integrated attenuator. The reaction product was monitored by periodical sampling of the gas phase from the glass chamber by using a gas-tight syringe and analyzed by GC (Varian GC-450) with a thermal conductivity detector (TCD, connected to a molecular sieve column) to detect H₂, O₂, and N₂ and a flame ionization detector (FID, connected to a CP-SIL 5CB capillary column) to detect hydrocarbons. Ar was used as the GC carrier gas. A methanizer was installed to enable the FID to detect CO with 1000× higher sensitivity. For the isotope-tracer experiment, the same photocatalytic procedure was used. After the addition of Cu₂O/RGO (0.5 g) into CO₂-saturated water (10 mL), the septum-sealed reactor was purged by Ar gas for 10 min. Then, ¹³CO₂ (¹³C 99%, Sigma-Aldrich) was introduced. The sample was irradiated with a 150 W Xe lamp for 30 min, and then 0.5 mL of the reaction product taken from the vessel headspace was analyzed by GC-MS (Shimadzu QP-2010SE) with a molecular sieve 5 Å capillary column. He gas was used as carrier gas during the measurement.

Acknowledgements

X.A. and J.T. acknowledge financial support from the European Commission under the 7th Framework Energy Program (Project reference: 309636). K.L. and J.T. are also thankful for a grant from the Qatar National Research Fund under its National Priorities Research Program award number NPRP 09-328-2-122. The contents of this paper are solely the responsibility of the authors and do not necessarily represent the official views of the Qatar National Research Fund.

Keywords: carbon · copper · graphene · photosynthesis · reduction

- [1] S. Habisreutinger, L. Schmidt-Mende, J. Stolarczyk, *Angew. Chem. Int. Ed.* **2013**, *52*, 7372–7408; *Angew. Chem.* **2013**, *125*, 7516–7557.
- [2] T. Inoue, A. Fujishima, S. Konishi, K. Honda, *Nature* **1979**, *277*, 637.
- [3] J. Tang, J. Durrant, D. Klug, *J. Am. Chem. Soc.* **2008**, *130*, 13885–13891.
- [4] J. Tang, A. Cowan, J. Durrant, D. Klug, *J. Phys. Chem. C* **2011**, *115*, 3143–3150.
- [5] S. Navalón, A. Dhakshinamoorthy, M. Alvaro, H. Garcia, *ChemSusChem* **2013**, *6*, 562–577.
- [6] M. Wang, L. Sun, Z. Lin, J. Cai, K. Xie, C. Lin, *Energy Environ. Sci.* **2013**, *6*, 1211–1220.
- [7] A. Paracchino, N. Mathews, T. Hisatomi, M. Stefik, S. Tilley, M. Grätzel, *Energy Environ. Sci.* **2012**, *5*, 8673–8681.
- [8] P. Tran, L. Wong, J. Barbercd, J. Loo, *Energy Environ. Sci.* **2012**, *5*, 5902–5918.
- [9] G. Ghadimkhani, N. Tacconi, W. Chanmanee, C. Janakyab, K. Rajeshwar, *Chem. Commun.* **2013**, *49*, 1297–1299.
- [10] A. Handoko, J. Tang, *Int. J. Hydrogen Energy* **2013**, *38*, 13017–13022.
- [11] A. Paracchino, V. Laporte, K. Sivula, M. Grätzel, E. Thimsen, *Nat. Mater.* **2011**, *10*, 456–461.
- [12] B. Li, T. Liu, L. Hu, Y. Wang, *J. Phys. Chem. Solids* **2013**, *74*, 635–640.
- [13] Z. Zhang, R. Dua, L. Zhang, H. Zhu, H. Zhang, P. Wang, *ACS Nano* **2013**, *7*, 1709–1717.
- [14] W. Tu, Y. Zhou, Q. Liu, S. Yan, S. Bao, X. Wang, M. Xiao, Z. Zou, *Adv. Funct. Mater.* **2013**, *23*, 1743–1749.
- [15] P. Wang, Y. Bai, P. Luo, J. Liu, *Catal. Commun.* **2013**, *38*, 82–85.
- [16] X. Lv, W. Fu, C. Hu, Y. Chen, W. Zhou, *RSC Adv.* **2013**, *3*, 1753–1757.
- [17] Y. Liang, B. Vijayan, K. Gray, M. Hersam, *Nano Lett.* **2011**, *11*, 2865–2870.
- [18] P. Tran, S. Batabyal, S. Pramana, J. Barber, L. Wong, S. Loo, *Nanoscale* **2012**, *4*, 3875–3878.
- [19] J. Lee, K. You, C. Park, *Adv. Mater.* **2012**, *24*, 1084–1088.
- [20] N. Li, Y. Xiao, C. Hu, M. Cao, *Chem. Asian J.* **2013**, *8*, 1960–1965.
- [21] X. An, J. Yu, F. Wang, C. Li, Y. Li, *Appl. Catal. B* **2013**, *129*, 80–88.
- [22] X. An, J. C. Yu, Y. Wang, Y. Hu, X. Yu, G. Zhang, *J. Mater. Chem.* **2012**, *22*, 8525–8531.
- [23] X. Qiu, M. Miyachi, K. Sunada, M. Minoshima, M. Liu, Y. Lu, D. Li, Y. Shimodaira, Y. Hosogi, Y. Kuroda, K. Hashimoto, *ACS Nano* **2012**, *6*, 1609–1618.
- [24] H. Liu, J. Wang, X. M. Fan, F. Z. Zhang, H. R. Liu, J. Dai, F. M. Xiang, *Mater. Sci. Eng.* **2013**, *178*, 158–166.
- [25] Z. Wang, Y. Liu, W. Wang, W. Huang, D. Martin, J. Tang, *Phys. Chem. Chem. Phys.* **2013**, *15*, 14956–14960.
- [26] A. Bazzo, A. Urakawa, *ChemSusChem* **2013**, *6*, 2095–2102.
- [27] S. Yan, S. Ouyang, J. Gao, M. Yang, J. Feng, X. Fan, L. Wan, Z. Li, J. Ye, Y. Zhou, Z. Zou, *Angew. Chem.* **2010**, *122*, 6544–6548.
- [28] K. Maeda, K. Sekizawa, O. Ishitani, *Chem. Commun.* **2013**, *49*, 10127–10129.
- [29] S. Sato, T. Morikawa, T. Kajino, O. Ishitani, *Angew. Chem. Int. Ed.* **2013**, *52*, 988–992; *Angew. Chem.* **2013**, *125*, 1022–1026.
- [30] Y. Zhang, Z. Tang, X. Fu, Y. Xu, *ACS Nano* **2010**, *4*, 7303–7314.
- [31] X. Lv, W. Fu, H. Chang, H. Zhang, J. Cheng, G. Zhang, Y. Song, C. Hu, J. Li, *J. Mater. Chem.* **2012**, *22*, 1539–1546.
- [32] C. Guo, H. Yang, Z. Sheng, Z. Lu, Q. Song, C. Li, *Angew. Chem. Int. Ed.* **2010**, *49*, 3014–3017; *Angew. Chem.* **2010**, *122*, 3078–3081.
- [33] W. Wang, J. Park, P. Biswas, *Catal. Sci. Technol.* **2011**, *1*, 593.
- [34] X. An, J. Yu, J. Tang, *J. Mater. Chem. A* **2014**, *2*, 1000–1005.
- [35] Y. Hsu, C. Yu, Y. Chen, Y. Lin, *J. Power Sources* **2013**, *242*, 541–547.
- [36] Y. Qiu, K. Yan, H. Deng, S. Yang, *Nano Lett.* **2012**, *12*, 407–413.
- [37] Y. Hsua, C. Yua, Y. Chen, Y. Lin, *Electrochim. Acta* **2013**, *105*, 62–68.
- [38] G. Katsukis, J. Malig, C. Schulz-Drost, S. Leubner, N. Jux, D. Guldi, *ACS Nano* **2012**, *6*, 1915–1924.
- [39] Y. Hou, A. Laursen, J. Zhang, G. Zhang, Y. Zhu, X. Wang, S. Dahl, I. Chorkendorff, *Angew. Chem. Int. Ed.* **2013**, *52*, 3621–3625; *Angew. Chem.* **2013**, *125*, 3709–3713.
- [40] B. Li, H. Cao, G. Yin, Y. Lu, J. Yin, *J. Mater. Chem.* **2011**, *21*, 10645–10648.
- [41] Q. Xiang, J. Yu, *J. Phys. Chem. Lett.* **2013**, *4*, 753–759.
- [42] W. Tu, Y. Zhou, Q. Liu, Z. Tian, J. Gao, X. Chen, H. Zhang, J. Liu, Z. Zou, *Adv. Funct. Mater.* **2012**, *22*, 1215–1221.
- [43] L. Jia, D. Wang, Y. Huang, A. Xu, H. Yu, *J. Phys. Chem. C* **2011**, *115*, 11466–11473.
- [44] C. Xiang, G. Kimball, R. Grimm, B. Brunshwig, H. Atwater, N. Lewis, *Energy Environ. Sci.* **2011**, *4*, 1311–1318.
- [45] W. Hummers, R. Offeman, *J. Am. Chem. Soc.* **1958**, *80*, 1339–1339.
- [46] Q. Zhai, S. Xie, W. Fan, Q. Zhang, Y. Wang, W. Deng, Y. Wang, *Angew. Chem. Int. Ed.* **2013**, *52*, 5776–5779; *Angew. Chem.* **2013**, *125*, 5888–5891.

Received: November 7, 2013

Revised: December 18, 2013

Published online on February 26, 2014